Applied Catalysis B: Environmental 238 (2018) 557–567

Contents lists available at ScienceDirect

Applied Catalysis B: Environmental

journal homepage: www.elsevier.com/locate/apcatb

A superior active and stable spinel sulfide for catalytic peroxymonosulfate oxidation of bisphenol S

Haodan Xu[a,b], Da Wang[a], Jun Ma[a,*], Tao Zhang[b], Xiaohui Lu[a], Zhiqiang Chen[a,*]

[a] State Key Laboratory of Urban Water Resource and Environment, School of Environment, Harbin Institute of Technology, Harbin, 150090, China
[b] Research Center for Eco-Environmental Sciences, Chinese Academy of Sciences, Beijing, 100085, China

ARTICLE INFO

Keywords:
Heterogeneous
Catalysis
Carrollite
Peroxymonosulfate
Bisphenol S
Sulfate radical

ABSTRACT

In this paper, for the first time the spinel sulfide carrollite ($CuCo_2S_4$) was applied to activate peroxymonosulfate (PMS) for the abatement of an endocrine disrupting compound (EDC) bisphenol S (BPS) in water. The hydrothermally synthesized $CuCo_2S_4$ outperformed conventional cobalt and copper oxides/sulfides in both catalytic activity and stability (i.e. metal leaching) in this oxidation process. The spinel sulfide was most active under neutral pH conditions, which is preferred for water/wastewater treatment. Sulfate radicals ($SO_4\cdot^-$) which was proved to be the prominent oxidant species in this oxidation process, attacked on BPS producing multiple hydroxylated degradation intermediates. Cu(II)/Cu(I) and Co(III)/Co(II) synergetic surface redox couples are found responsible for the catalytic activation of PMS producing $SO_4\cdot^-$; furthermore, the thermodynamically favorable reaction between surface Cu(I) and surface Co(III) guarantees the electron transfer between the surface metal sites. As confirmed by turnover frequency calculation, $CuCo_2S_4$ has higher catalytic effect per surface cobalt atom than the counterpart oxides for PMS activation, probably due to the lower electronegativity of S^{2-} than O^{2-}. $CuCo_2S_4$ could be a potentially useful catalyst for water/wastewater treatment.

1. Introduction

Bisphenols are widely used in consumer products like polycarbonate plastics and epoxy resins. Some of them are categorized as endocrine disrupting compounds (EDCs), thus being environmental concerns [1]. Since bisphenol A (BPA) was found toxic and banned in many countries [2], alternative analogues such as bisphenol S (BPS; 4,4′-sulfonyldiphenol), bisphenol B (BPB; 2,2′-bis(4-hydrox-yphenyl)butane), bisphenol F (BPF; 4,4′-dihydroxydiphenylmethane), and bisphenol AF (BPAF; 4,4′-(hexafluoroisopropylidene)diphenol) gradually gained their popularity in application [3,4]. As a result, BPS has been detected in human urine [5], canned foodstuffs [6] and environmental samples like indoor dust and sewage sludge [7,8]. Unfortunately, BPS has acute toxicity towards antiandrogenic activity [9] and estrogenic activity [10]. According to a recent report, parental exposure to environmentally relevant concentrations of BPS can cause delayed and damaged hatching of zebrafish as well as malformation of offspring [11].

Various methods have been tested to remove bisphenols from water, and advanced oxidation processes (AOPs) are considered to be efficient for the detoxification of bisphenols [12,13]. Currently, most AOPs are based on the generation of free radicals such as hydroxyl radicals (·OH) [14], superoxide radicals ($O_2\cdot^-$) [15] and sulfate radicals ($SO_4\cdot$-) [16]. In the past few years, sulfate radical-based AOPs where the radicals are produced via activation of peroxymonosulfate (PMS, $KHSO_5$) or persulfate (PS, $K_2S_2O_8$) attracted many research interests. PMS usually can be dissociated by various catalysts more easily than PS due to its asymmetric structure, i.e. $HO\text{-}OSO_3^-$ vs $^-_3OSO\text{-}OSO_3^-$ [17,18].

Ionic cobalt (Co^{2+}) has been recognized as the most efficient homogeneous catalyst for PMS activation, but its application is quite limited because of the toxicity of this ion [19]. To minimize the side-effects of ionic cobalt, cobalt-based heterogeneous catalysts like cobalt oxides [20,21] and cobalt-containing multi-metal oxides [22,23] were further investigated. Mineral spinels with general formula AB_2X_4, where A and B are metal cations and X is chalcogen (O, S, Se, Te), often exhibit remarkable electrical, magnetic and other physical properties [24,25]. The high activity of spinel ferrites in activating PMS to remove recalcitrant organic pollutants has been well studied [26,27]. Several spinel cobaltites where cobalt took the B-sites were also reported to be effective for PMS activation [28,29].

Most of the research focused on transition metal spinel oxides. In the meantime, spinel sulfides also received research interests. Rather than

* Corresponding author.
E-mail addresses: xhdhit2016@163.com (H. Xu), wangdahit@126.com (D. Wang), majun@hit.edu.cn, majunhit@126.com (J. Ma), taozhang@rcees.ac.cn (T. Zhang), 879260488@qq.com (X. Lu), czqhit@163.com (Z. Chen).

https://doi.org/10.1016/j.apcatb.2018.07.058
Received 11 May 2018; Received in revised form 5 July 2018; Accepted 21 July 2018
Available online 21 July 2018

environmental applications, transition metal sulfides with spinel structures known as thiospinels are prominent materials for lithium ion batteries [30] and supercapacitors [31] where metal oxides have been conventionally employed, owing to their high electric conductivity and electrochemical activity. Thiospinels were also investigated as bi-functional catalysts for oxygen evolution reactions (OER) [32], oxygen reduction reactions (ORR) [33] and hydrogen generation/evolution reactions [34]. Copper cobalt sulfide spinel carrollite ($CuCo_2S_4$), mainly exposed with (111) planes, is a stable electrocatalyst of OER in alkaline medium [35]. Unlike some spinel oxides which can only be artificially synthesized, carrollite deposits can be found as natural mineral [36]. In spite of the extensive research on sulfide spinel for above mentioned functions, to the best of our knowledge, the performance and mechanism of carrollite-catalyzed AOPs have not been reported yet. Though mackinawite (FeS) [37] and magnetic pyrrhotite ($Fe_{1-x}S$) [38] have been studied as heterogeneous catalysts in AOPs, massive metal ion leaching was always a big problem associated with the transformation of sulfide species, which implies that the catalytic efficiency cannot be guaranteed in long term of operation. Bimetallic spinel sulfides could be rather stable under various conditions, thus being worthy of investigation as environmental catalysts.

In this work, we tested $CuCo_2S_4$ for catalytic activation of PMS to generate sulfate radicals. $CuCo_2S_4$ of hierarchical structures were prepared and their morphological and physicochemical properties were characterized. BPS was selected as a model pollutant to evaluate the catalytic performance of $CuCo_2S_4$ in comparison to other sulfides and oxides. Influences of different experimental parameters in $CuCo_2S_4$ catalytic PMS system were tested. The mechanism was investigated with a series of instrument characterization including X-ray diffraction (XRD), X-ray photoelectron spectroscopy (XPS) and electron paramagnetic resonance (EPR). Stability of the catalyst and degradation pathways of BPS were also evaluated.

2. Materials and methods

2.1. Chemicals and reagents

BPS, Oxone (PMS, $KHSO_5{\cdot}0.5KHSO_4{\cdot}0.5K_2SO_4$), tert-butanol (TBA), thiourea and CuS powder were purchased from Aladdin Chemical Reagent Co., Ltd., China. Cobalt nitrate hexahydrate ($Co(NO_3)_2{\cdot}6H_2O$), copper nitrate trihydrate ($Cu(NO_3)_2{\cdot}3H_2O$), cobalt chloride hexahydrate ($CoCl_2{\cdot}6H_2O$), copper chloride bihydrate ($CuCl_2{\cdot}2H_2O$), ethylenediamine, sodium thiosulfate ($Na_2S_2O_3$), 2,2-azino-bis(3-ethylbenzothiazoline)-6-sulfonic acid (ABTS) and 5,5-dimethyl-1-pyrolin-*N*-oxide (DMPO) were obtained from Sigma-Aldrich, USA. Methanol (MeOH), acetic acid and acetonitrile were purchased from Tedia, USA. Other chemicals of analytical grade or better were purchased from Aladdin Chemical Reagent Co., Ltd., China and used as received. All solutions were prepared using pure water (Milli-Q, 18.2 MΩ cm) produced from purification system (Millipore, USA).

2.2. Catalysts preparation and characterization

The thiospinel nanosheets were synthesized via a modified hydrothermal procedure [35]. In a typical preparation, $Co(NO_3)_2{\cdot}6H_2O$ and $Cu(NO_3)_2{\cdot}3H_2O$ at a molar ratio of 2:1 were first dissolved in 120 mL pure water, and then stirred for 10 min. to form a homogeneous pink solution. Adequate amount of thiourea was then slowly introduced to this solution with vigorous stirring for another 15 min. With addition of 8 mL of ethylenediamine, the solution instantly became dark brown, forming obvious precipitates. The suspension was then transferred to a 200 mL Teflon-lined autoclave, sealed and kept at 200 °C for 16 h. After cooling to ambient temperature, the as-obtained black product was washed with pure water and ethanol for several times and dried at 70 °C overnight. Other sulfides were synthesized following similar procedure. Adding Co salt alone produced cobalt sulfide (named Co_xS_y). To investigate the influence of solvent on crystal formation, the pure water was replaced by 120 mL of glycol in preparation. The solid obtained in this way is represented as g-$CuCo_2S_4$. $CuCo_2S_4$-Cl was prepared with cobalt chloride and copper chloride under the same condition as $CuCo_2S_4$. To probe the influence of hydrothermal reaction time, $CuCo_2S_4$ samples were synthesized at 200 °C for 12 and 20 h, which were noted as $CuCo_2S_4$-12 and $CuCo_2S_4$-20 respectively. Detailed preparation of metal oxides Co_3O_4 and $CuCo_2O_4$ can be found in Text S1, Supporting Information (SI).

X-ray diffraction (XRD) patterns were acquired from a diffractometer (max-TTR-III, Rigaku D, Japan) with Cu-Kα radiation source at 45 kV and 40 mA. X-ray photoelectron spectroscopy (XPS) was conducted using a photoelectron spectrometer (ESCALAB 250Xi, Thermo Scientific, USA) equipped with a dual X-ray source using Al-Kα. Field emission scanning electron microscopy (FE-SEM) (SIGMA500, Zeiss, Germany) equipped with an energy dispersive X-ray (EDX) detector system was performed to obtain the surface morphology and elemental composition information. Morphology and crystal structures were further analyzed using high-resolution transmission electron microscopy (HR-TEM) (JEM-2100, JEOL, Japan). Specific surface area and pore structures were determined using Brunauer-Emmett-Teller (BET) and Barrett-Joyner-Halenda (BJH) models based on nitrogen adsorption-desorption isotherm measurements at −196 °C on a surface area and porosity analyzer (ASAP 2020, Micromeritics, USA). Zeta potential was measured on Zetasizer Nano-ZS90 (Malvern, USA).

2.3. Experimental procedures

Batch experiments were conducted in 250 mL flasks at 25 °C water bath with magnetic stirring. Solution pH was controlled with 5 mM phosphate buffer, guaranteeing that the variation of pH was below ± 0.2 during experiments. Although phosphate ions might affect the performance of catalyst, it has better buffer capacity at near neutral pH than the commonly used borate buffer. In pre-experiment we compared phosphate and borate both of 5 mM for the reaction at initial pH 7.2 (data not shown). The degradation rates were nearly the same in 30 min. reaction under the experimental condition; moreover, the pH variance was within 0.1 in the phosphate buffered reaction solution, while it was within 0.4 in the borate buffered one. Reactions were initiated by simultaneous addition of catalyst and PMS into buffered solution of the target compound. At desired time intervals 1 mL of water sample was collected and filtered through a glass fiber filter of 0.22 μm pore size. The residual oxidant was quenched with 1 M $Na_2S_2O_3$ solution for BPS analysis. The filter had no impact on the residual BPS and PMS concentration.

For reusability tests, the first run was conducted for a volume of 1000 mL reaction solution at the catalyst dose of 20 mg with other conditions the same as the control experiment. After reaction, the remaining catalyst in the solution was recovered with centrifugation and then washed with pure water. It was further dried out at 70 °C overnight and weighted 16 mg for the second run of 800 mL solution. For each run the reaction solution was reduced by 200 mL volume while maintaining the mass concentration of the catalyst (0.01 g L^{-1}) in the reaction solution.

2.4. Analytical methods

A Waters 2487 HPLC equipped with dual λ UV–vis detector and Symmetry C18 column (4.6 mm × 150 mm, 5 μm) was used for BPS and other target compounds analysis. The mobile phase consisted of 0.1% (v/v%) acetic acid solution and methanol at volume of 50:50 (v/v%) flow rate of 1 mL min^{-1}. Concentrations of PMS stock solution and residual PMS were analyzed by iodometric method [39]. Cobalt and copper leaching during the experiments were quantified on inductively coupled plasma-optical emission spectrometry (ICP-OES) (7300, Perkin Elmer, USA). Degradation intermediates and products of BPS were

analyzed with LC–QTOF-MS/MS (X500, AB Sciex, USA) at ESI negative ionization mode. The injection volume of each sample solution was 20 μL. The gradient mobile phase of pure water (A) and acetonitrile (B) was maintained at 0.5 mL min^{-1} flow rate. The gradient was as follows: 0 min (5% B), 5 min (5% B), 15 min (95% B), 25 min (95% B), 30 min (5% B) and 35 min (5% B). The ionization source parameters were as follows: spray voltage, 5500 V; source temperature, 500 °C; curtain gas, ion source gas 1 and ion source gas 2 were set at 35, 50 and 50 psi. The mass scan was collected from *m/z* 100–800 Da in negative ionization mode for both MS and MS/MS. A typical information-dependent acquisition (IDA) operation mode was applied for MS/MS detection. PMS was added to buffered solution with pre-mixed catalyst and spin-trapping agent DMPO and then the reaction solution was measured on EPR spectrometer (EMX-8/2.7, Bruker, Germany) at certain time intervals under the following conditions: X-field sweep; center field, 3475.00 G; sweep width, 80.00 G; frequency, 9.7 GHz; power, 40.50 mW; scan time, 20.5 s; scan number, 10 times.

3. Results and discussion

3.1. Characterization of catalysts

Powder XRD spectra of as-synthesized samples (Fig. 1a) show that all the $CuCo_2S_4$ samples have similar XRD pattern. The peaks of $CuCo_2S_4$ centered at 16.14°, 26.63°, 31.36°, 38.01°, 46.99°, 50.09° and 54.84° are in good agreement with (111), (022), (113), (004), (224), (115) and (044) phases, all of which match for carrollite structured $CuCo_2S_4$ according to the JCPDS card No. 42-1450. When the hydrothermal reaction time in preparation was reduced to 12 h, the as-obtained product $CuCo_2S_4$-12 contains Co_9S_8 and CoS impurities and has lower crystallinity. The extension of hydrothermal reaction to 20 h led to over oxidation and formation of CoS. As shown in Fig. S1a (SI), XRD patterns of g-$CuCo_2S_4$ show the presence of Co_4S_3, Co_9S_8, CoS and CoS_2, indicating that glycol is not an appropriate solvent to prepare carrollite. XRD patterns of $CuCo_2S_4$-Cl also reveal the presence of CoS_2 and CoS. Therefore, nitrate metal precursors and hydrothermal reaction of 16 h were applied to prepare relatively pure and well-crystalized $CuCo_2S_4$. The sample Co_xS_y consists of CoS, Co_9S_8 and CoS_2, among which CoS is the main constituent. Relatively pure $CuCo_2O_4$ and Co_3O_4 were also successfully prepared, the XRD patterns of which were indexed to JCPDS card No. 001-1155 and No. 009-0418, respectively (Fig. S1b, SI).

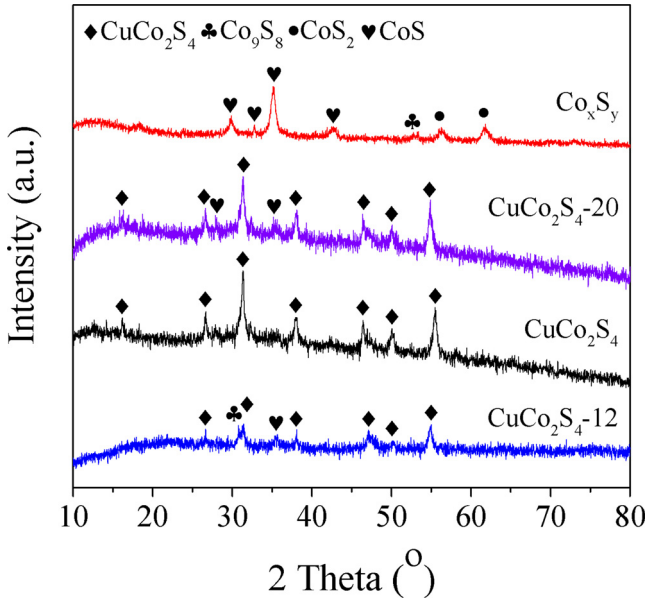

Fig. 1. XRD patterns of as-synthesized metal sulfides.

The near-surface elemental proportions and chemical states of $CuCo_2S_4$ were analyzed by high resolution XPS spectra as displayed in Fig. 2. The survey spectrum in Fig. 2a shows the presence of Co, Cu, S, C and O. The C 1s at 285.0 eV identified as adventitious carbon can be used to correct the shift of binding energy. The deconvolution of Co 2p core level spectrum show two spin-orbit doublets and two shakeup satellites in Fig. 2b. The two prominent peaks at 778.6 eV and 793.6 eV correspond to Co $2p_{3/2}$ and Co $2p_{1/2}$ with the spin-energy separation of approximate 15 eV both fitting with two spin-orbit doublets, confirming the co-existence of Co(III) and Co(II) oxidation state [31,40]. The feature of 780.9 eV and 795.6 eV doublets indicates a strong Co-S interaction [33]. Similar type of Co 2p spectrum is observed in Co_xS_y sample (Fig. S2, SI), but the higher intensity of 778.6 eV and 793.6 eV peaks in Fig. 2b underscores much larger amount of octahedral Co(III) on the surface of $CuCo_2S_4$. In Fig. 3c the two peaks at 932.3 eV and 952.2 eV fit well with Cu $2p_{3/2}$ and Cu $2p_{1/2}$ spin-orbit doublets, which can be assigned to both Cu(I) and Cu(II), respectively [41]. The satellite peaks which represent metal-ligand charge transfer further attest the presence of Cu(II) at octahedral sites [42]. As shown in Fig. 2d, the binding energies of the S $2p_{3/2}$ and S $2p_{1/2}$ peaks are 161.3 eV and 163.8 eV, indicating that most of the S species exist as S^{2-}. The peak at 162.4 eV corresponds to typical metal-sulfur bonding (Cu−S and Co−S bonding) [43]. The other peak at 168.4 eV can be attributed to adsorbed oxygen on S forming sulfate-like species. As this peak has relatively low intensity, the amount of the sulfate-like species should be quite limited on the surface of $CuCo_2S_4$ [31]. The oxygen species is adsorbed oxygen impurity rather than lattice oxygen, which can be removed by in situ Ar^+ sputter cleaning, a method reported in the literature [35]. This assumption is supported by the XRD spectrum (Fig. 1) which shows no metal oxide peaks. The elemental ratio of Cu, Co and S is found to be 14.12:26.72:59.16 according to XPS analysis, close to the theoretical value of 1:2:4.

The nitrogen adsorption-desorption isotherms and pore size distribution of the samples were presented in Fig. S3b (SI). $CuCo_2S_4$ has specific surface area of 12.769 $m^2 g^{-1}$ with the average pore size of 25.9 nm, and Fig. S2b (SI) indicates a hierarchical mesopore/macropore structure of $CuCo_2S_4$. Further morphology characterizations with FE-SEM and HR-TEM are presented in Fig. 3. As shown in Fig. 3a and b, the 3D hierarchical structure of $CuCo_2S_4$ with the size of 1–2 μm was formed by interconnected nanoflakes [35] (Fig. 3c). Both the flat surfaces and lateral sides were exposed, and the lattice fringes corresponding to (111) (d = 0.548 nm), (022) (d = 0.334 nm), (113) (d = 0.286 nm), and (004) (d = 0.236 nm) phases are recognized in Fig. 3d. This is also confirmed in XRD patterns (Fig. 1). EDX elemental mapping images in Fig. S4 (SI) exhibit the uniform presence of Cu, Co, and S in $CuCo_2S_4$ particles. Fig. S5a (SI) shows that the size of $CuCo_2S_4$-12 in hierarchical structure is similar to the optimized sample, but there were many tiny nanoscale particles stacked on the edge of nanoflakes, possibly due to inadequate hydrothermal time. As for $CuCo_2S_4$-20 in Fig. S5b (SI), the size of nanostructure obviously shrunk and fragments emerged, suggesting the collapse of nanoflakes caused by over hydrothermal procedure. Lattice fringes of (111) and (113) are also observed in $CuCo_2S_4$-12 and $CuCo_2S_4$-20; besides, the 0.259 and 0.292 nm lattice fringes representing (002) (Fig. S5c, d, SI) and (100) (Fig. S5d, SI) phases further verify the existence of CoS (Jaipurite) as Fig. 1 suggests.

3.2. PMS activation by $CuCo_2S_4$ for BPS degradation

The catalytic efficiency of $CuCo_2S_4$ for PMS activation was compared with other cobalt sulfides and oxides. As illustrated in Fig. 4, the BPS adsorption on $CuCo_2S_4$ surface was indiscernible, and PMS alone degrade only 10% BPS in 30 min. Other catalysts also had little BPS adsorption (data not shown). $CuCo_2S_4$/PMS coupled oxidation achieved complete BPS degradation within 30 min, in comparison to 42%, 70% and 72% BPS degradation by PMS activated by CuS, Co_3O_4 and $CuCo_2O_4$, respectively. The catalytic activity of $CuCo_2S_4$-12, $CuCo_2S_4$-

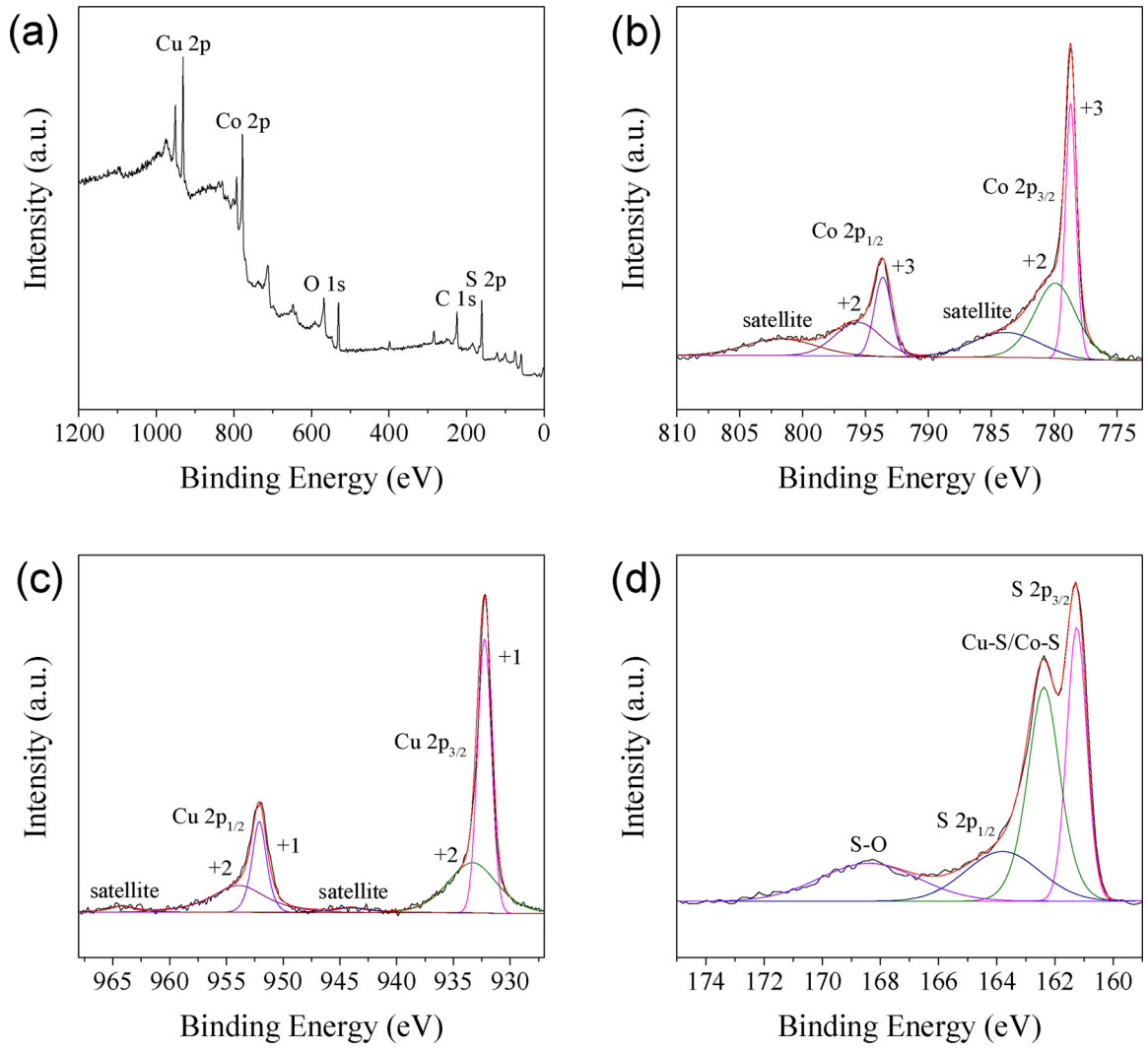

Fig. 2. (a) Wide scan XPS survey spectrum and high-resolution (b) Co 2p, (c) Cu 2p and (d) S 2p XPS spectra of as-synthesized $CuCo_2S_4$.

20 and $CuCo_2S_4$ were basically identical. $CuCo_2S_4$-Cl, g-$CuCo_2S_4$ and Co_xS_y exhibited even higher activity than $CuCo_2S_4$ in this process (Fig. S6, SI), which is probably due to their higher Co^{2+} leaching during the reaction (Fig. S7, SI). Co^{2+} leaching from $CuCo_2S_4$ was nearly an order of magnitude lower than Co_xS_y, owing to its superior structure as bi-metallic sulfide spinel. For this reason, $CuCo_2S_4$ was selected for further detailed study.

3.2.1. Kinetics

With excess PMS dosage (100–400 μM) the degradation rate of BPS fitted well with pseudo-first order reaction model. The logarithm of the observed degradation rate of BPS (k_{obs}) was linearly correlated with that of the initial PMS dosage (insert graph in Fig. 5a). The decomposition rate of PMS was independent on the BPS concentration (Fig. 5b). PMS decomposition was linearly correlated to that of catalyst $CuCo_2S_4$ dosage. Based on these results, the overall reaction rate r of this heterogeneous catalyst oxidation can be expressed in Eq. (1), where k represents the overall apparent reaction rate constant, and α, β, and γ are reaction orders related to concentrations of PMS, BPS and $CuCo_2S_4$, respectively. As determined in above experiments, α, β, and γ are 0.610, 0 and 0.652 respectively, while $k = 0.086\ min^{-1}$ is obtained through Eq. (2) with data in Fig. 5c. The overall reaction rate has an order of 1.26 (i.e., α + β + γ).

$$r = \frac{-d[BPS]}{dt} = \frac{-d[PMS]}{dt} = k[PMS]^{\alpha}[BPS]^{\beta}[CuCo2S4]^{\gamma} \quad (1)$$

$$\frac{-d[PMS]}{dt} = k[PMS]^{0.610}[CuCo2S4]^{0.652} = k_{obs}[PMS] \quad (2)$$

3.2.2. Identification of reactive species

$SO_4\cdot^-$ and ·OH usually are main reactive species generated during catalytic PMS activation [44]. Radical scavengers, i.e. MeOH and TBA, were used to distinguish respective radicals, as MeOH with three α-H readily reacts with both $SO_4\cdot^-$ and ·OH ($k_{SO4\cdot-/MeOH} = 2.5 \times 10^7\ M^{-1}\ s^{-1}$, $k_{\cdot OH/MeOH} = 9.7 \times 10^8\ M^{-1}\ s^{-1}$) while TBA without α-H reacts with ·OH much faster than with $SO_4\cdot^-$ ($k_{SO4\cdot-/TBA} = 4.0–9.1 \times 10_5\ M^{-1}\ s^{-1}$, $k_{\cdot OH/TBA} = 3.8–7.6 \times 10^8\ M^{-1}\ s^{-1}$) [45]. As shown in Fig. 6a, TBA had a minor impact on BPS degradation, while MeOH significantly inhibited this reaction. The initial rate constants in Table S1 (SI) illustrate the scavenging effects quantitatively. It is noteworthy that with excess MeOH, the BPS degradation nearly ceased after the initial stage (Fig. 6a). It is estimated that sulfate radicals contributed about 95% BPS degradation under this condition of catalytic oxidation.

The radicals were further confirmed on EPR after reaction with DMPO, a spin trapping reagent. Signals of DMPO-OH and DMPO-SO_4 adducts were both detected based on their hyperfine splitting constants (DMPO-OH: $\alpha_H = 14.8$, $\alpha_N = 14.8$; DMPO-SO_4: $\alpha_H = 9.6$, $\alpha_H = 1.48$, $\alpha_H = 0.78$, $\alpha_N = 13.2$). Fig. 6b reveals that the DMPO-OH signals

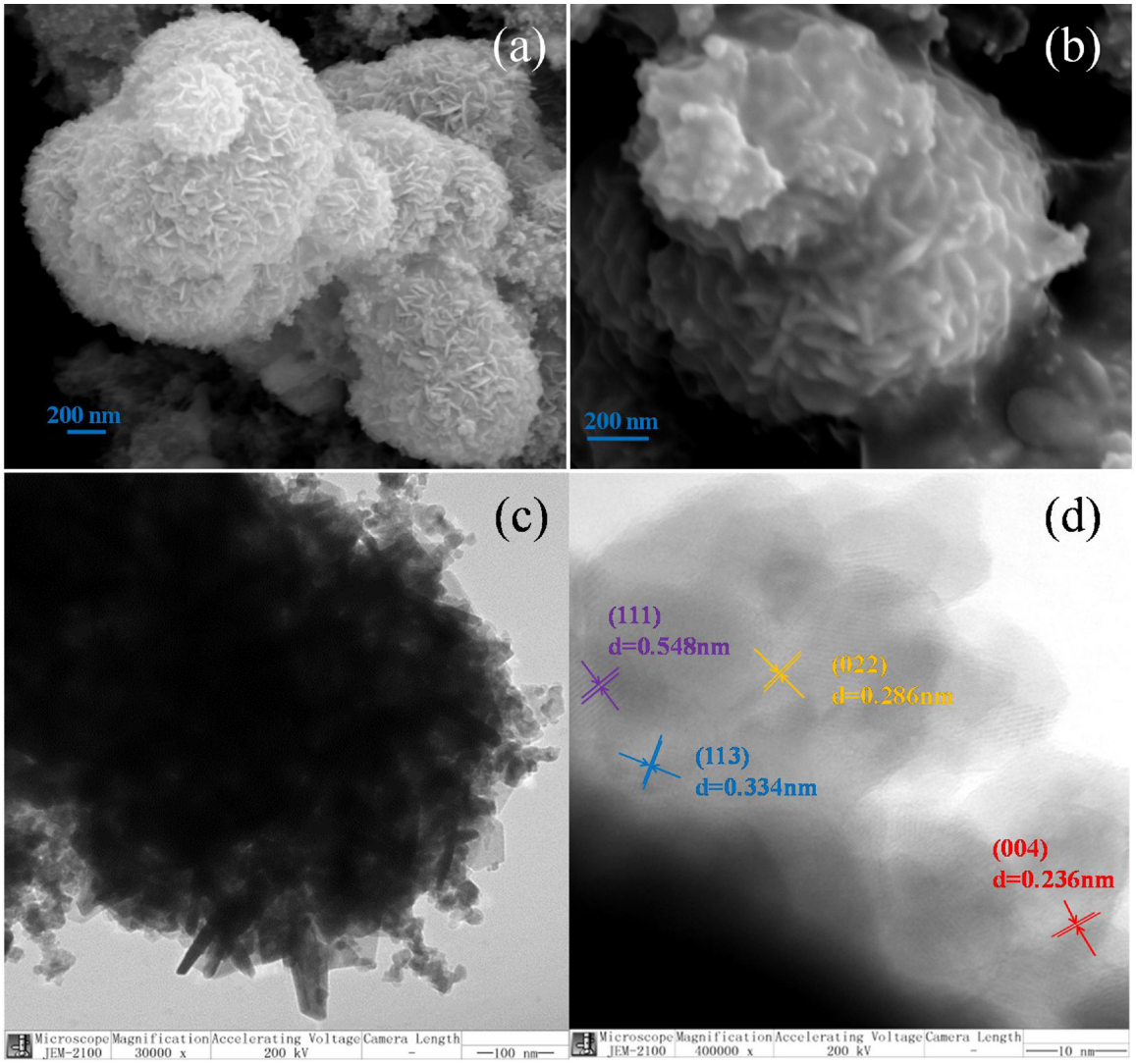

Fig. 3. FE-SEM images (a, b) of $CuCo_2S_4$ interconnected nanosheets and HR-TEM images (c, d) of $CuCo_2S_4$ including some clear lattice fringes.

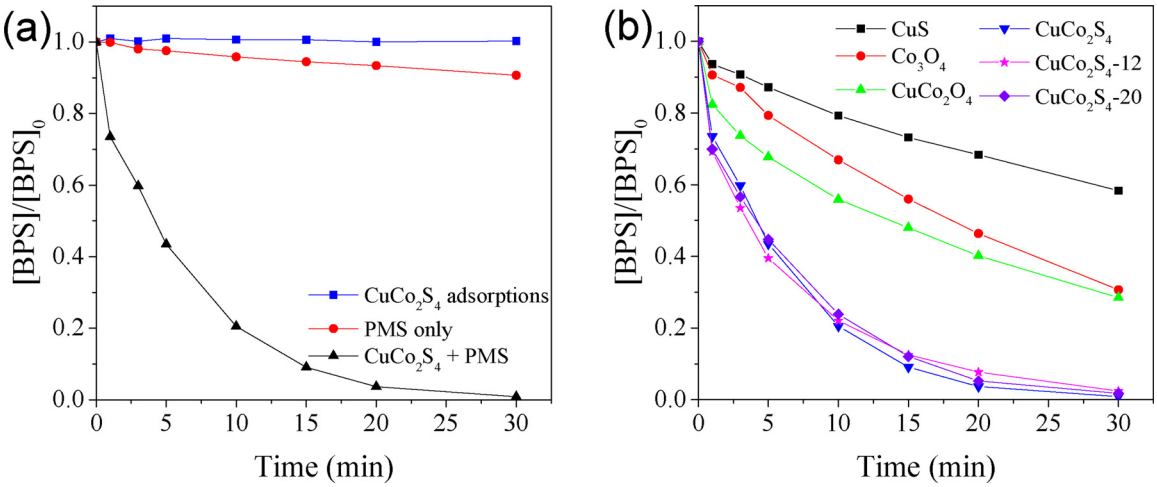

Fig. 4. (a) BPS removal by $CuCo_2S_4$ adsorption, PMS and PMS/$CuCo_2S_4$; (b) Comparison of different as-synthesized metal sulfides or oxides for catalytic BPS oxidation ([catalyst] = 0.01 g L^{-1}, $[BPS]_0$ = 10 μM, $[PMS]_0$ = 100 μM, pH = 7.2, T = 25 °C).

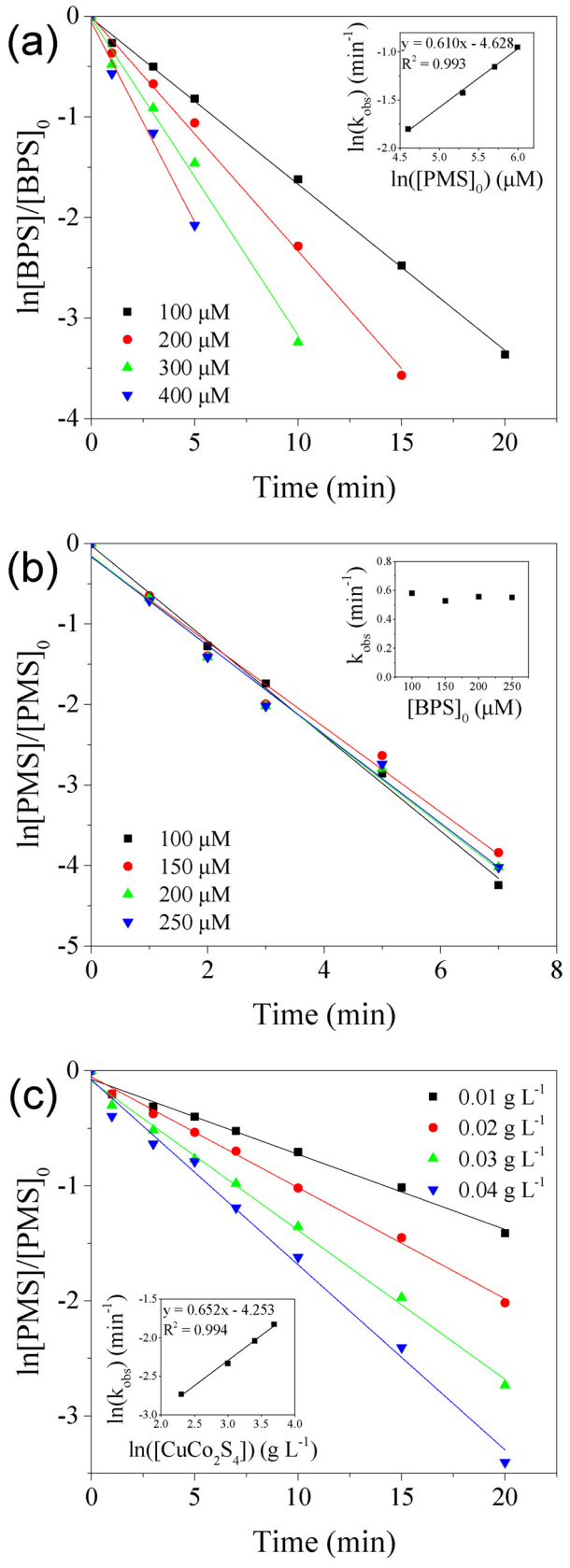

Fig. 5. (a) Influence of PMS dose on BPS decomposition ($[CuCo_2S_4]$ = 0.01 g L^{-1}, $[BPS]_0$ = 10 μM, pH = 7.2, T = 25 °C), (b) influence of BPS dose on PMS decomposition ($[CuCo_2S_4]$ = 0.01 g L^{-1}, $[PMS]_0$ = 50 μM, pH = 7.2, T = 25 °C) and (c) influence of $CuCo_2S_4$ dose on PMS decomposition ($[BPS]_0$ = 10 μM, $[PMS]_0$ = 100 μM, pH = 7.2, T = 25 °C).

increased in the first 10 min. and then decreased. Signals of DMPO-SO_4 are much lower than DMPO-OH. The DMPO-SO_4 adduct possibly was transformed into DMPO-OH through rapid nucleophilic substitution by H_2O/OH^- as depicted in Scheme S1 (SI) [46]. But still both $SO_4\cdot^-$ and ·OH were detected in the presence of $CuCo_2S_4$, while neither of them was monitored in the system with only DMPO and PMS/DMPO (Fig. S8, SI).

As depicted in Fig. S9a (SI), 0.01 g L^{-1} $CuCo_2S_4$ and 100 μM PMS resulted in 20% TOC removal after 30 min. The low mineralization efficiency was due to inadequate oxidant dosage because the TOC removal tripled at PMS dosage of 300 μM. Interestingly, unlike BPS degradation the TOC removal cannot be fitted with the pseudo-first order reaction model, but shows a plateau phase from 5 to 10 min followed by a rapid increase between 10 to 20 min. This results indicates that some degradation intermediates of BPS probably react with $SO_4\cdot^-$ faster than the parent compound for mineralization.

Lutze et al. reported that the cleavage of the *N*-ethyl group was largely favored over the cleavage of the *N*-isopropyl group in the reaction of atrazine with $SO_4\cdot^-$, while the difference is not so remarkable in the case of ·OH [44]. The formation of two degradation products of atrazine, desethyl-atrazine (DEA) and desisopropyl-atrazine (DIA), thereby can be used to differentiate the contributions of the two radical species in the reaction. The reported DEA/DIA molar ratio is about 10 for $SO_4\cdot^-$ induced degradation of atrazine; in contrast, the ratio is about 3 for ·OH-dominated atrazine degradation [44,47]. Fig. S9b (SI) exhibits the generation of DEA and DIA during PMS/$CuCo_2S_4$ oxidation of atrazine. The ratio of yield DEA to DIA was about 8.5. This result further confirms the major role of $SO_4\cdot^-$ in the $CuCo_2S_4$ catalyzed PMS oxidation.

3.2.3. Influence of experimental conditions

3.2.3.1. Influence of solution pH. pH usually significantly influences the performance of heterogeneous catalytic reactions in water. Fig. 7a shows the variation of BPS degradation within the pH range of 5.1–9. $CuCo_2S_4$ was most active under slightly acidic condition (pH 6.1–7.2), and the reactivity decreased when the solution was acidic or alkaline. The surface of $CuCo_2S_4$ was negatively charged under all pH conditions in this experiment (Fig. S10, SI). Fig. S11 (SI) shows PMS decomposition under these pHs, the trend of which is in consistence with BPS degradation. The intense adverse effect of H^+ towards both BPS degradation and PMS decomposition means that the PMS activation was hindered, which was also found in other PMS/PDS activation processes at low pHs [48,49]. Since the pK_{a1} and pK_{a2} of BPS are 7.42 and 8.03 respectively [50], the compound is deprotonated at 8.1 and 9.0. The rapid decline of BPS removal over pH 7 is partly due to self-decomposition of PMS at a higher pH [51] and lower redox potential of reactive species (i.e. $^1O_2$ and $O_2\cdot^-$) produced in base-activated PMS [52]. The proportion of SO_5^{2-} increases with pH (PMS has a $pK_{a1} < 0$ and a pK_{a2} = 9.4), which probably leads to reduced electro-static interaction of PMS with the negatively-charged surface of $CuCo_2S_4$ particles [26]. This assumption is confirmed by the decreased PMS decomposition at alkaline pH. Moreover, sulfate radicals will be converted to hydroxyl radicals (Eq. (3)) under alkaline condition. The second order rate constant of ·OH with BPS is calculated to be 9.03×10^7 M^{-1} s^{-1} [53], which is rather slow considering that the second order rate constants of ·OH and many other organic pollutants are usually around 10^9 M^{-1} s^{-1} [54].

$$SO_4\cdot^- + OH^- \rightarrow SO_4^{2-} + \cdot OH \qquad k = 6.5 \times 10^7\ M^{-1}\ s^{-1} \qquad (3)$$

3.2.3.2. Influence of temperature. The solution temperature strongly influences PMS/$CuCo_2S_4$ oxidation of BPS (Fig. 7b). The k_{obs} value increased from 0.086 min^{-1} to 0.444 min^{-1} as the temperature was raised from 15 °C to 45 °C. The correlation between pseudo-first order reaction rate constant and temperature was depicted via Arrhenius

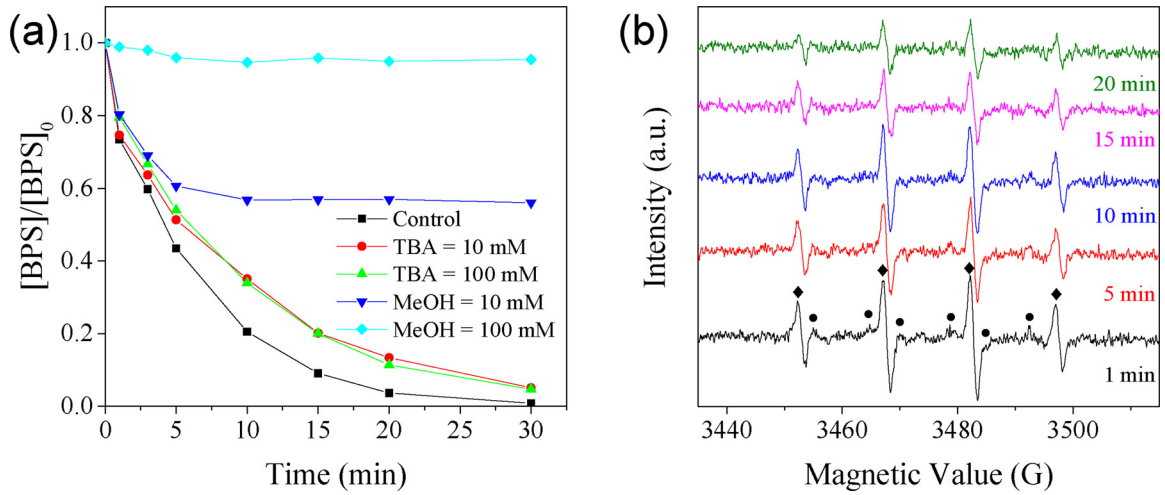

Fig. 6. (a) Effect of quenching agents on PMS/$CuCo_2S_4$ oxidation ([catalyst] = 0.01 g L^{-1}, $[BPS]_0$ = 10 μM, $[PMS]_0$ = 100 μM, pH = 7.2, T = 25 °C); (b) EPR spectra of $CuCo_2S_4$ catalyzed PMS activation: (♦) DMPO − OH and (●) DMPO-SO_4 ([catalyst] = 0.5 g L^{-1}, $[PMS]_0$ = 1.5 mM, $[DMPO]_0$ = 40 mM, pH = 7.2, T = 25 °C).

equation (Eq. (4)) where E_a is the activation energy, R is the universal gas constant (8.314 J mol^{-1} K^{-1}) and A is a constant. The activation energy of BPS degradation by PMS/$CuCo_2S_4$ oxidation can be obtained by plotting $\ln k_{obs}$ vs 1000/T.

$$\ln k_{obs} = \ln A - E_a/RT \quad (4)$$

E_a is 40.67 kJ mol^{-1} for this reaction, which is lower than that of

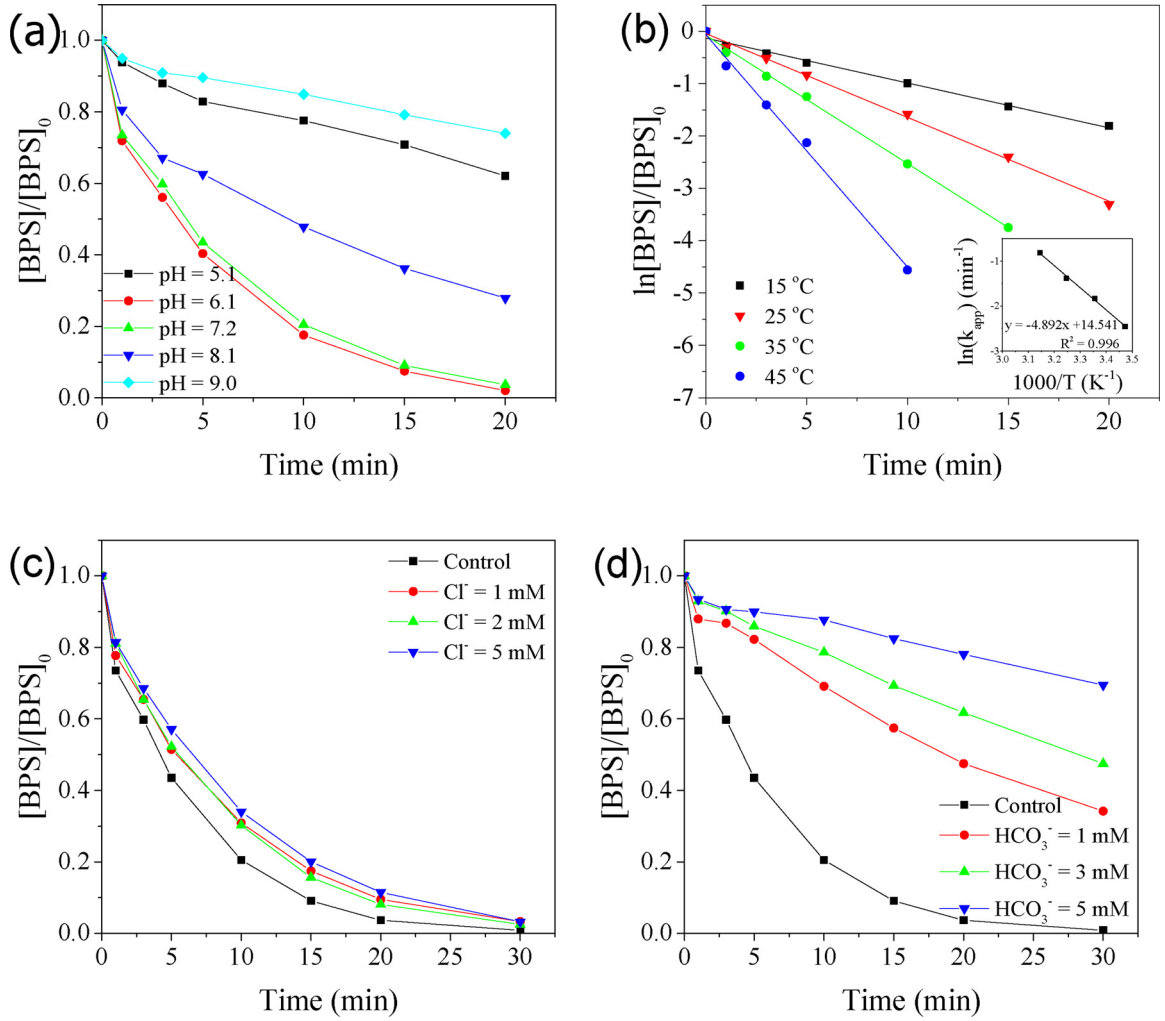

Fig. 7. Effect of (a) solution pH ([catalyst] = 0.01 g L^{-1}, $[BPS]_0$ = 10 μM, $[PMS]_0$ = 100 μM, T = 25 °C), (b) temperature ([catalyst] = 0.01 g L^{-1}, $[BPS]_0$ = 10 μM, $[PMS]_0$ = 100 μM, pH = 7.2), (c) chloride and (d) bicarbonate ([catalyst] = 0.01 g L^{-1}, $[BPS]_0$ = 10 μM, $[PMS]_0$ = 100 μM, pH = 7.2, T = 25 °C) on PMS/$CuCo_2S_4$ degradation of BPS.

PMS oxidation activated by Fe_2O_3 [55] and supported cobalt oxides [56,57], suggesting that $CuCo_2S_4$ could be a promising catalyst under mild ambient temperature.

3.2.3.3. Influence of inorganic ions. Chloride is one of the dominant scavengers of $SO_4\cdot^-$ in water (Eq. (5) [54]. Several reactive species such as $Cl_2\cdot^-$ (2.09 V) and Cl_2 (1.36 V) can be generated during the chloride-sulfate radical reaction (Eqs. (6)–(13)) [54]. The presence of Cl^- thus influences activated PMS oxidation. The BPS removal by PMS/$CuCo_2S_4$ oxidation only slightly decreased when 1–5 mM Cl^- was added. The active chlorine species can react with BPS and prevent the recombination of sulfate radicals (Eq. (14)), thus does not influence BPS removal obviously. The minor influence of chloride on the reaction was also reported for PMS/$CuFe_2O_4$ system [26].

$$SO_4\cdot^- + Cl^- \rightarrow SO_4^{2-} + Cl\cdot \quad k = 3.0 \times 10^8\ M^{-1}\ s^{-1} \tag{5}$$

$$SO_4^{2-} + Cl\cdot \rightarrow SO_4\cdot- + Cl^- \quad k = 2.5 \times 10^8\ M^{-1}\ s^{-1} \tag{6}$$

$$Cl\cdot + H_2O \rightarrow ClOH\cdot^- + H^+ \quad k = 2.5 \times 10^5\ M^{-1}\ s^{-1} \tag{7}$$

$$ClOH\cdot^- + H^+ \rightarrow Cl\cdot + H_2O \quad k = 2.1 \times 10^{10}\ M^{-1}\ s^{-1} \tag{8}$$

$$ClOH\cdot^- + Cl^- \rightarrow Cl_2\cdot^- + OH- \quad k = 1.0 \times 10^4\ M^{-1}\ s^{-1} \tag{9}$$

$$Cl\cdot + OH^- \rightarrow ClOH\cdot- \quad k = 1.8 \times 10^{10}\ M^{-1}\ s^{-1} \tag{10}$$

$$Cl\cdot + Cl^- \rightarrow Cl_2\cdot- \quad k = 8.5 \times 10^9\ M^{-1}\ s^{-1} \tag{11}$$

$$Cl_2\cdot^- + Cl\cdot \rightarrow Cl_2 + Cl- \quad k = 2.1 \times 10^9\ M^{-1}\ s^{-1} \tag{12}$$

$$Cl\cdot + Cl\cdot \rightarrow Cl_2 \quad k = 8.8 \times 10^7\ M^{-1}\ s^{-1} \tag{13}$$

$$SO_4\cdot^- + SO_4\cdot^- \rightarrow S_2O_8^{2-} \quad k = 7.0 \times 10^8\ M^{-1}\ s^{-1} \tag{14}$$

Bicarbonate is another natural scavenger which reacts with $SO_4\cdot^-$ very fast (Eq. (15)). As shown in Fig. 7d, the BPS degradation rate declined to 66% in the presence of HCO_3^- (1 mM). The degradation rate further declined to 31% when 5 mM of HCO_3^- was added. The inhibitory function of HCO_3^- was mainly due to its reaction with $SO_4\cdot^-$ to form $HCO_3\cdot^-$ (1.65 V), a radical species with low reactivity [58].

$$SO_4\cdot^- + HCO_3^- \rightarrow HCO_3\cdot + SO_4^{2-} \quad k = 2.8 \times 10^6\ M^{-1}\ s^{-1} \tag{15}$$

3.2.4. Stability and reusability of $CuCo_2S_4$

For sustainable application purposes, the stability and reusability of the heterogeneous catalyst are highly desired. Therefore, a reusability test of $CuCo_2S_4$ was conducted (results are shown in Fig. 8a). In five repeated runs, almost 100% BPS removal was achieved in 30 min. Unlike some other catalysts [59], it seems there was clearly no activity decline for the $CuCo_2S_4$ catalyst. XRD spectra in Fig. S12 (SI) confirms that the $CuCo_2S_4$ maintained carrollite crystal structure after repeated using.

Metal ion leaching from the catalyst at different pHs was monitored by ICP-OES. Generally, both Co and Cu leaching decreased with the increase of pH (Fig. 8b). About 0.036 mg L^{-1} of Co and 0.032 mg L^{-1} of Cu ions were leached from $CuCo_2S_4$ at a dosage of 0.01 g L^{-1} and neutral pH. The metal leaching is quite low compared with some reported perovskite catalysts [59,60]. To illustrate the contribution of leached metal ions, the filtrate of a control experiment without taking out samples was collected and used as buffered homogeneous catalyst solution. As shown in Fig. 8c, the pseudo-first-order reaction rate constant of leached metal ions catalytic process was only 0.063 min^{-1} (for $CuCo_2S_4$ catalysis is 0.158 min^{-1}), proving that $CuCo_2S_4$ heterogeneous catalysis oxidation dominates BPS degradation.

3.2.5. Mechanism of PMS activation by $CuCo_2S_4$

The mechanisms of PMS activation by perovskite/spinel oxide are usually proposed through the study of valence states of transition metals before and after using. For instance, it was proposed that PMS decomposes to sulfate radicals on CuO and $CuFe_2O_4$ due to the PMS reaction with Cu(I) on the surface [61,62]. To clarify how the $CuCo_2S_4$

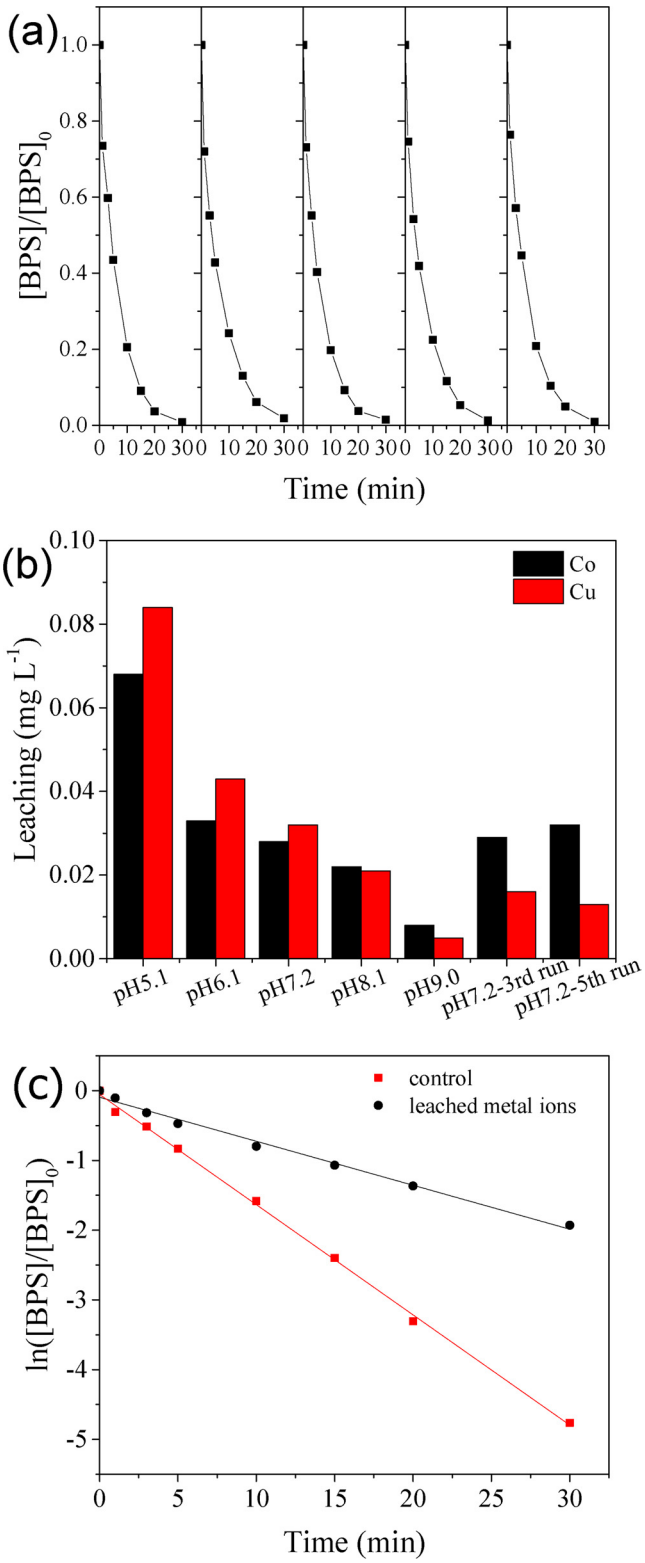

Fig. 8. (a) BPS degradation in different runs of PMS/$CuCo_2S_4$ oxidation ([catalyst] = 0.01 g L^{-1}, $[BPS]_0$ = 10 μM, $[PMS]_0$ = 100 μM, pH = 7.2, T = 25 °C); (b) Co and Cu cations leached in different reaction solutions ([catalyst] = 0.01 g L^{-1}, $[BPS]_0$ = 10 μM, $[PMS]_0$ = 100 μM, T = 25 °C, reaction time = 30 min.); (c) BPS degradation in the system of PMS/leached metal ions.

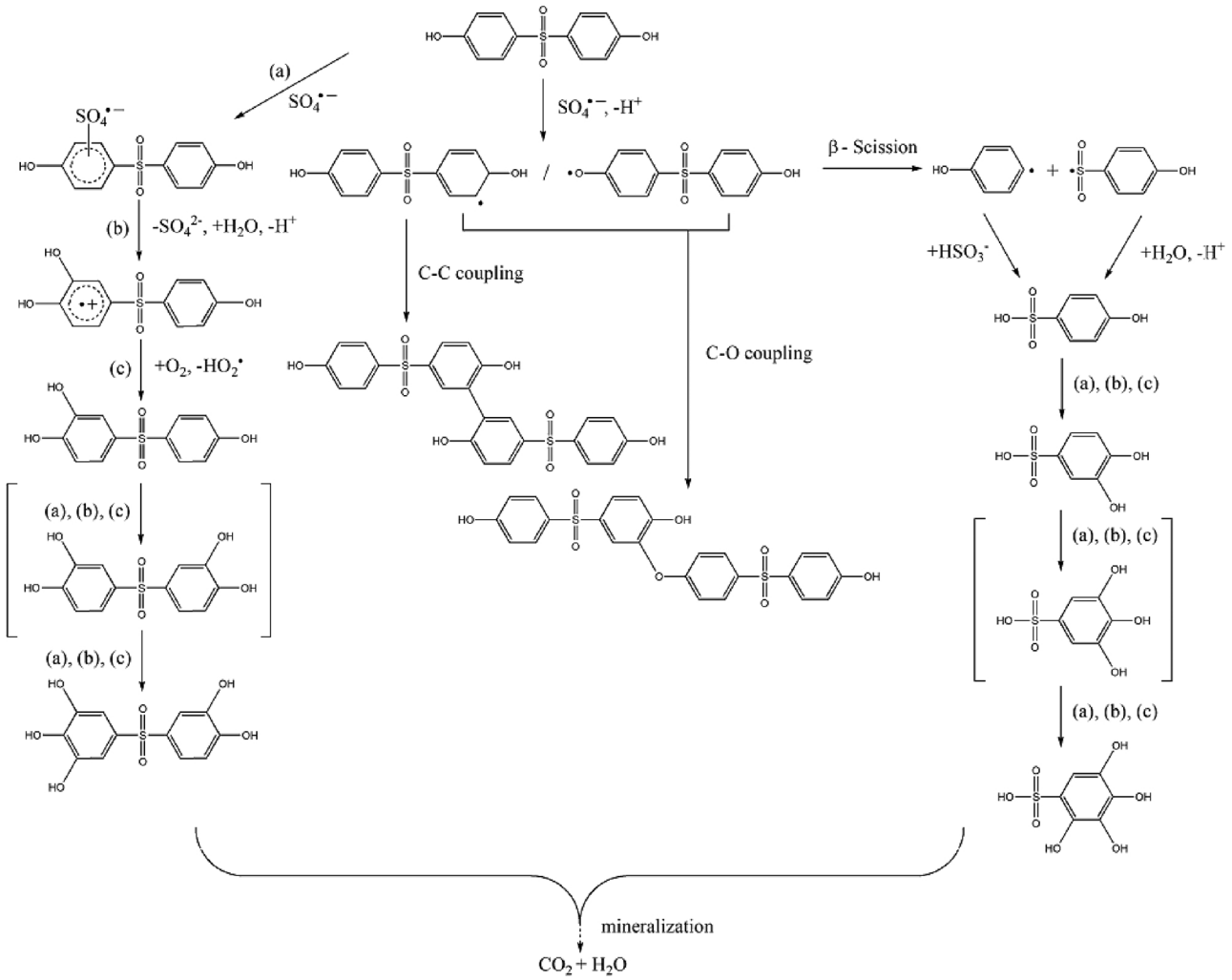

Fig. 9. Possible degradation pathways of BPS during PMS/$CuCo_2S_4$ oxidation.

catalyst functions during the PMS activation, high resolution XPS spectra of virgin and used $CuCo_2S_4$ were compared and displayed in Fig. S13 (SI). The main peaks of Co 2p and Cu 2p slightly shifted to higher binding energies after reaction, indicating the change in valence states. The ratio of Co(III)/Co(II) was 0.88 in virgin $CuCo_2S_4$, whereas the ratio of spent catalyst was 1.07, implying that electron transferred from cobalt to PMS during the activation. Correspondingly, the decrease in the ratio of Cu(I)/Cu(II) from 1.25 to 0.92 demonstrates that some Cu(I) was oxidized to Cu(II). According to this result and former studies, reactions involved in $CuCo_2S_4$ catalyzed activation of PMS can be depicted in following equations (due to the much lower reducing potential of $SO_5\cdot^-$ (1.10 V), the function of $SO_5\cdot^-$ was not taken into account in this study):

$$\equiv Cu(I) + HSO_5^- \rightarrow \equiv Cu(II) + SO4\cdot- + OH- \quad (16)$$

$$\equiv Cu(II) + HSO5- \rightarrow \equiv Cu(I) + SO5\cdot- + H+ \quad (17)$$

$$\equiv Cu(I) + \equiv Co(III) \rightarrow \equiv Cu(II) + \equiv Co(II) \quad (18)$$

$$\equiv Co(III) + HSO5- \rightarrow \equiv Co(II) + SO5\cdot- + H+ \quad (19)$$

$$\equiv Co(II) + HSO5- \rightarrow \equiv Co(III) + SO4\cdot- + OH- \quad (20)$$

The appearance of Cu(I) and Co(III) in virgin $CuCo_2S_4$ supports the conclusion of Buckley et al., that carrollite can be represented by $Cu^{(I)}Co_2^{(III)}(S_4)^{(-VII)}$ [63]. Reactions of Eqs. (16)–(20) consequently guarantee the unfailing activation of PMS by $CuCo_2S_4$, and Eq. (18) which is thermodynamically favorable ($E_{Co(III)/Co(II)}$ = 1.84 V, $E_{Cu(II)/Cu(I)}$ = 0.15 V) proposes the synergistic relationship of the two metal sites in $CuCo_2S_4$.

Turnover frequency (TOF), an intrinsic factor characterizing the catalyst performance, can be estimated by several parameters of a catalyst and the specific reaction involved. TOF of as-synthesized Co_3O_4, $CuCo_2O_4$ and $CuCo_2S_4$ catalysts were evaluated to be 1.31, 0.57 and 5.87 × 10^{-3} s^{-1} (details of calculation were presented in Test S2, SI). Therefore, the TOF of $CuCo_2S_4$ was 5 and 10 fold greater than the two cobalt oxides. Binary cobalt sulfides were reported to have much lower optical band gap energy and much higher conductivity compared to corresponding oxides [64]. The substitution of oxygen with sulfur would create a more flexible structure because of lower electronegativity of sulfur [43]. Besides, binary transition metal sulfides possess richer redox active sites and correspondingly better electrochemical activity than mono-metal sulfides [65].

3.2.6. BPS degradation pathways and intermediates

It has been demonstrated that $SO_4\cdot^-$ is the major oxidant species in PMS/$CuCo_2S_4$ oxidation of BPS. The electrophilic $SO_4\cdot^-$ usually reacts with organic compounds through electron abstraction [66]. $SO_4\cdot^-$ reacts with functional groups in the preference order of aromatic > $-CH_2$ > $-CO$ > $-COOH$ and reacts with benzene ring via H-abstraction forming carbon center radicals [67]. In previous studies degradation pathways of both BPA [68] and BPS [69] attacked by sulfate radicals were discussed. Though the structure of the two bisphenols differs, some of the degradation intermediates were alike for identical reaction

mechanisms.

A total of six degradation intermediates were detected and identified with LC-QTOF-MS/MS analysis, all of which are listed in Table S2 (SI). Based on these degradation intermediates, the degradation pathway of BPS is proposed (Fig. 9). $SO_4\cdot^-$ reacts with the aromatic ring of BPS, forming short-lived sulfate radical adducts (lifetime < 200 ns, step (a)) [70]. Nucleophilic attack by water occurs on the as-formed sulfate radical adducts (step (b)), which also can be completed via electron abstraction mechanism [71]. Oxygen or PMS further reacts with hydroxylated BPS radical to form monohydroxylated BPS (step (c)) [72]. The hydroxylation primarily occurs at the *ortho* position of the −OH group due to the substituent orientation effect. The monohydroxylated BPS further reacts with $SO_4\cdot^-$ through steps (a)–(c) producing bi- and trihydroxylated BPS.

Hydrogen abstraction by $SO_4\cdot^-$ occurs on phenolic hydroxyl group or aromatic ring producing BPS radicals. Bimolecular combination of BPS radicals through C—C or C—O coupling produces two isomers with higher molecular weight [73]. Meanwhile, β-Scission on the BPS radicals forms phenoxy and 4-hydroxybenzenesulfinate radicals. 4-Hydroxybenzenesulfonic acid is produced via hydroxylation of 4-hydroxybenzenesulfinate radicals and the addition of sulfite ions to phenolic radicals. This product is attacked by $SO_4\cdot^-$ and reacts through steps (a)–(c) to form multi-hydroxylated benzenesulfonic acids.

4. Conclusions

$CuCo_2S_4$ shows high activity and stability in catalytic activation of PMS for BPS oxidation and is superior to other copper and cobalt chalcogen compounds. The PMS/$CuCo_2S_4$ oxidation process is most effective near neutral pH (6.1–7.2), under which condition metal leaching is relatively low. Sulfate radical is the main reactive species in this process. The sulfate-radical attack on BPS produces mainly hydroxylated intermediates. The redox circles of surface Cu(I)/Cu(II) and Co(II)/Co(III) on $CuCo_2S_4$ are mainly responsible for PMS activation; the sulfide spinel probably has more redox reactive sites than oxide, accounting for higher TOF of $CuCo_2S_4$ than the corresponding oxide.

Acknowledgements

This work was financially supported by the National Key Research and Development Program (2017YFA0207203, 2016YFC0401107 and 2016YFB0600502) and the Funds of the Major Science and Technology Program for Water Pollution Control and Treatment (2017ZX07201003-03).

Appendix A. Supplementary data

Supplementary material related to this article can be found, in the online version, at doi:https://doi.org/10.1016/j.apcatb.2018.07.058.

References

[1] Q. Husain, S. Qayyum, Crit. Rev. Biotechnol. 33 (2013) 260–292.
[2] D. Chen, K. Kannan, H. Tan, Z. Zheng, Y.L. Feng, Y. Wu, M. Widelka, Environ. Sci. Technol. 50 (2016) 5438–5453.
[3] M.Y. Chen, M. Ike, M. Fujita, Environ. Toxicol. 17 (2002) 80–86.
[4] S. Kitamura, T. Suzuki, S. Sanoh, R. Kohta, N. Jinno, K. Sugihara, S.I. Yoshihara, N. Fujimoto, H. Watanabe, S. Ohta, Toxicol. Sci. 84 (2005) 249–259.
[5] C. Liao, F. Liu, H. Alomirah, V.D. Loi, M.A. Mohd, H.B. Moon, H. Nakata, K. Kannan, Environ. Sci. Technol. 46 (2012) 6860–6866.
[6] P. Viñas, N. Campillo, N. Martínez-Castillo, M. Hernández-Córdoba, Anal. Bioanal. Chem. 397 (2010) 115–125.
[7] C. Liao, F. Liu, Y. Guo, H.B. Moon, H. Nakata, Q. Wu, K. Kannan, Environ. Sci. Technol. 46 (2012) 9138–9145.
[8] X. Yu, J. Xue, H. Yao, Q. Wu, A.K. Venkatesan, R.U. Halden, K. Kannan, J. Hazard. Mater. 299 (2015) 733–739.
[9] E. Grignard, S. Lapenna, S. Bremer, Toxicol. In Vitro 26 (2012) 727–731.
[10] S. Kitamura, T. Suzuki, S. Sanoh, R. Kohta, N. Jinno, K. Sugihara, S. Yoshihara, N. Fujimoto, H. Watanabe, S. Ohta, Toxicol. Sci. 84 (2005) 249–259.
[11] K. Ji, S. Hong, Y. Kho, K. Choi, Environ. Sci. Technol. 47 (2013) 8793–8800.
[12] C. Wang, L. Zhu, C. Song, G. Shan, P. Chen, Appl. Catal. B: Environ. 105 (2011) 229–236.
[13] X. Wang, Y. Qin, L. Zhu, H. Tang, Environ. Sci. Technol. 49 (2015) 6855–6864.
[14] C. Lee, J. Yoon, U. Von Gunten, Water Res. 41 (2007) 581–590.
[15] J. Shi, Z. Ai, L. Zhang, Water Res. 59 (2014) 145–153.
[16] Y. Ren, L. Lin, J. Ma, J. Yang, J. Feng, Z. Fan, Appl. Catal. B: Environ. 165 (2015) 572–578.
[17] N.J.D. Graham, Environ. Sci. Technol. 41 (2007) 613–619.
[18] R.H. Waldemer, P.G. Tratnyek, R.L. Johnson, J.T. Nurmi, Environ. Sci. Technol. 41 (2007) 1010–1015.
[19] G.P. Anipsitakis, D.D. Dionysiou, Environ. Sci. Technol. 38 (2004) 3705–3712.
[20] G.P. Anipsitakis, E. Stathatos, D.D. Dionysiou, J. Phys. Chem. B 109 (2005) 13052–13055.
[21] K.H. Chan, W. Chu, Water Res. 43 (2009) 2513–2521.
[22] Q. Yang, H. Choi, S.R. Al-Abed, D.D. Dionysiou, Appl. Catal. B: Environ. 88 (2009) 462–469.
[23] Y. Feng, D.L. Wu, Y. Deng, T. Zhang, K.M. Shih, Environ. Sci. Technol. 50 (2016) 3119–3127.
[24] N.W. Grimes, Phys. Technol. 6 (1975) 22–27.
[25] K.E. Sickafus, J.M. Wills, N.W. J. Am. Ceram. Soc. 82 (2004) 3279–3292.
[26] T. Zhang, H. Zhu, J.P. Croué, Environ. Sci. Technol. 47 (2013) 2784–2791.
[27] T. Zhang, Y. Chen, T. Leiknes, Environ. Sci. Technol. 50 (2016) 5864–5873.
[28] Y. Feng, J. Liu, D. Wu, Z. Zhou, Y. Deng, T. Zhang, K. Shih, Chem. Eng. J. 280 (2015) 514–524.
[29] X. Tian, C. Tian, Y. Nie, C. Dai, C. Yang, N. Tian, Z. Zhou, Y. Li, Y. Wang, Chem. Eng. J. 331 (2018) 144–151.
[30] W. Wei, L. Mi, Y. Gao, Z. Zheng, W. Chen, X. Guan, Chem. Mater. 26 (2014) 3418–3426.
[31] J. Tang, Y. Ge, J. Shen, M. Ye, Chem. Commun. (Camb.) 52 (2016) 1509–1512.
[32] M. Shen, C. Ruan, Y. Chen, C. Jiang, K. Ai, L. Lu, ACS Appl. Mater. Interfaces 7 (2015) 1207–1218.
[33] J. Kibsgaard, Z. Chen, B.N. Reinecke, T.F. Jaramillo, Nat. Mater. 11 (2012) 963–969.
[34] L. Yu, B.Y. Xia, X. Wang, X.W. Lou, Adv. Mater. 28 (2016) 92–97.
[35] M. Chauhan, K.P. Reddy, C.S. Gopinath, S. Deka, ACS Catal. 7 (2017) 5871–5879.
[36] A.E. Annels, D.J. Vaughan, J.R. Craig, Miner. Depos. 18 (1983) 71–88.
[37] J. Fan, L. Gu, D. Wu, Z. Liu, Chem. Eng. J. 333 (2018) 657–664.
[38] D. Xia, Y. Li, G. Huang, R. Yin, T. An, G. Li, H. Zhao, A. Lu, P.K. Wong, Water Res. 112 (2017) 236–247.
[39] R.E. Ball, J.O. Edwards, M.L. Haggett, P. Jones, J. Am. Chem. Soc. 89 (1967) 2331–2333.
[40] H. Zhu, J. Zhang, R. Yanzhang, M. Du, Q. Wang, G. Gao, J. Wu, G. Wu, M. Zhang, B. Liu, J. Yao, X. Zhang, Adv. Mater. 27 (2015) 4752–4759.
[41] K. Roy, C.S. Gopinath, Anal. Chem. 86 (2014) 3683–3687.
[42] M.R. Gao, Y.F. Xu, J. Jiang, Y.R. Zheng, S.H. Yu, J. Am. Chem. Soc. 134 (2012) 2930–2933.
[43] W. Hu, R. Chen, W. Xie, L. Zou, N. Qin, D. Bao, ACS Appl. Mater. Interfaces 6 (2014) 19318–19326.
[44] H.V. Lutze, S. Bircher, I. Rapp, N. Kerlin, R. Bakkour, M. Geisler, C. Von Sonntag, T.C. Schmidt, Environ. Sci. Technol. 49 (2015) 1673–1680.
[45] P. Neta, R.E. Huie, A.B. Ross, J. Phys. Chem. Ref. Data 17 (1988) 1027–1284.
[46] G.S. Timmins, K.J. Liu, E.J.H. Bechara, Y. Kotake, H.M. Swartz, Free Radic, Biol. Med. 27 (1999) 329–333.
[47] A. Tauber, C. Von Sonntag, Acta Hydrochim. Hydrobiol. 28 (2000) 15–23.
[48] Y.H. Guan, J. Ma, X.C. Li, J.Y. Fang, L.W. Chen, Environ. Sci. Technol. 45 (2011) 9308–9314.
[49] T. Zhang, Y. Chen, Y. Wang, J. Le Roux, Y. Yang, J.P. Croué, Environ. Sci. Technol. 48 (2014) 5868–5875.
[50] J. Regueiro, A. Breidbach, T. Wenzl, Rapid Commun. Mass Spectrom. 29 (2015) 1473–1484.
[51] Y.R. Wang, W. Chu, J. Hazard. Mater. 186 (2011) 1455–1461.
[52] C. Qi, X. Liu, J. Ma, C. Lin, X. Li, H. Zhang, Chemosphere 151 (2016) 280–288.
[53] HSDB: Bisphenol S, Toxnet, U.S. National Library of Medicine, 2012 (Accessed 19 October 2012), https://toxnet.nlm.nih.gov/cgi-bin/sis/search2/f?./temp/~cll7QW:3.
[54] Y. Yang, J.J. Pignatello, J. Ma, W.A. Mitch, Water Res. 89 (2016) 192–200.
[55] F. Ji, C. Li, X. Wei, J. Yu, Chem. Eng. J. 231 (2013) 434–440.
[56] P.R. Shukla, S. Wang, H. Sun, H.M. Ang, M. Tadé, Appl. Catal. B: Environ. 100 (2010) 529–534.
[57] W. Tian, H. Zhang, Z. Qian, T. Ouyang, H. Sun, J. Qin, M.O. Tadé, S. Wang, Appl. Catal. B: Environ. 225 (2018) 76–83.
[58] Z. Zuo, Z. Cai, Y. Katsumura, N. Chitose, Y. Muroya, Radiat. Phys. Chem. 55 (1999) 15–23.
[59] C. Su, X. Duan, J. Miao, Y. Zhong, W. Zhou, S. Wang, Z. Shao, ACS Catal. 7 (2017) 388–397.
[60] S.B. Hammouda, F. Zhao, Z. Safaei, V. Srivastava, D.L. Ramasamy, S. Iftekhar, S. Kalliola, M. Sillanpää, Appl. Catal. B: Environ. 215 (2017) 60–73.
[61] F. Ji, C. Li, L. Deng, Chem. Eng. J. 178 (2011) 239–243.
[62] Y. Ding, L. Zhu, N. Wang, H. Tang, Appl. Catal. B: Environ. 129 (2013) 153–162.
[63] A.N. Buckley, W.M. Skinner, S.L. Harmer, A. Pring, L.J. Fan, Geochim. Cosmochim. Acta 73 (2009) 4452–4467.
[64] H. Chen, J. Jiang, L. Zhang, H. Wan, T. Qi, D. Xia, Nanoscale 5 (2013) 8879–8883.
[65] S.E. Moosavifard, S. Fani, M. Rahmanian, Chem. Commun. (Camb.) 52 (2016) 4517–4520.
[66] C.L. Clifton, R.E. Huie, Int. J. Chem. Kinet. 21 (1989) 677–687.
[67] T. Ito, S. Morimoto, S. Fujita, S. Nishimoto, Radiat. Phys. Chem. 78 (2009)

256–260.
[68] L. Zhao, Y. Ji, D. Kong, J. Lu, Q. Zhou, X. Yin, Chem. Eng. J. 303 (2016) 458–466.
[69] Q. Wang, X. Lu, Y. Cao, J. Ma, J. Jiang, X. Bai, T. Hu, Chem. Eng. J. 328 (2017) 236–245.
[70] R.O.C. Norman, P.M. Storey, P.R. West, J. Chem. Soc. B: Phys. Org. (1970) 1087–1095.
[71] P. Neta, V. Madhavan, H. Zemel, R.W. Fessenden, J. Am. Chem. Soc. 99 (1977) 163–164.
[72] B. Darsinou, Z. Frontistis, M. Antonopoulou, I. Konstantinou, D. Mantzavinos, Chem. Eng. J. 280 (2015) 623–633.
[73] J. Sharma, I.M. Mishra, D.D. Dionysiou, V. Kumar, Chem. Eng. J. 276 (2015) 193–204.